CrystEngComm

Accepted Manuscript

ROYAL SOCIETY OF CHEMISTRY

www.rsc.org/crystengcomm

Construction about different fold interpenetrated POMOFs with the same topology

Liang Li [a,b], Jing-Wen Sun[a], Jing-Quan Sha[a*], Guang-Ming Li[a], Peng-Fei Yan[a*], Cheng Wang[a]

[a]*Key Laboratory of Functional Inorganic Material Chemistry (MOE), P. R. China; School of Chemistry and Materials Science, Heilongjiang University; Harbin 150080, P. R. China*

[b]*The Key Laboratory of Biological Medicine Formulation，Heilongjiang Provincial; School of Pharmacy, Jiamusi University, Jiamusi, 154007, PR China*

Abstract: Three different fold interpenetrated metal-organic networks based on Keggin-type polyoxometalates have been hydrothermally synthesized by a simple change in organic ligand and structurally characterized. By changing the length and coordination mode of ligand, compound **1** represents the first example of three-fold interpenetrated POMOF architecture with ***pcu*** topology, and POMs occupy the vertex of ***pcu*** lattice. Compound **2** exhibits a POM-pillared metal-organic framework, which can be described overall as two-fold interpenetrated ***pcu*** frameworks, and POMs occupy the arris of ***pcu*** lattice. Different from **1** and **2**, compound **3** can be described as a single ***pcu*** network and POMs occupy the face of ***pcu*** lattice. The influence of the organic ligand on the degree of interpenetration is also discussed. Furthermore, the results about the photocatalytic activities indicate that three compounds present good photocatalytic activities.

Keyword: Polyoxometalates /Metal-organic Frameworks/ Interpenetration; Photocatalytic activity

Introduction

Self-assembled combinations of well-designed molecular building blocks (MBBs) and organic ligands have attracted extensive attention of materials chemist and have afforded a wide range of metal-organic frameworks (MOFs) because of their intriguing structures and fascinating properties like gas absorption and catalysis.[1] Because such properties are primarily bound to structure, the control over structure is crucial.[2] From the synthetic point of view, polyoxometalates (POMs), as primarily soluble anionic metal oxide clusters, are suitable inorganic MBBs to combine with different transition-metal organic subunits, due to their discrete structures, biology, magnetism, materials science and catalysis properties. [3] Therefore, grafting POMs into MOFs can integrate both the properties of the MOFs and POMs in the same system, which can open up a new avenue for the creation of a variety of novel topologies and multifunctional POM-based metal-organic frameworks (POMOFs). [4]

Interpenetration system, one of the common characteristics in organic–inorganic hybrid compounds, has become more and more attractive because of their fascinating structures and special applications,[5] and many spectacular interpenetrated topologies were observed.[6] So many compounds with interpenetrated features have been targeted synthesized by changing temperature or concentration of reactant,[7] the type of anions in salts, [8] the organic ligands [9] and the template during the synthesis.[10] However, only a few examples about the POMOFs with interpenetrated structure were reported, [11] maybe due to the bigger size and the uncontrollable coordination geometry of POMs. Therefore, the study about the interpenetrated POMOFs remains a great challenging work. Note that recent studies show that the interpenetration is not quite so bad in many aspects. For example, theoretical calculations have predicted that non-interpenetrated structures should have better gas-sorption capacities than interpenetrated structures,[12] but Forster's group reported that interpenetrated structures showed higher gas-sorption capacities for N_2 and H_2 gases at 77 K under both low and high pressures, and at 298 K under high pressure in 2008. [10a] In 2012, Suh and coworkers also reported the interpenetrated structure exhibits generally much

higher gas adsorption capacities than the non-interpenetrated structure at low pressures.[10d] Despite these contradictory arguments, it is difficult to prove which one is the more general case, because property study should be compared among frameworks with similar structures that only differ in their degree of interpenetration, namely, there is a lack of a systematic study on how to control the interpenetration.

Based on the previous work and comprehensive consideration, and to obtain and control the interpenetrated folds of POMOF networks, we rely on the suitably designed structure and coordination mode of organic molecules as a general strategy for the preparation of target compounds. In this work, we select 4,4'-bipyridine (hereafter noted bipy), 1,4-bis(pyrid-4-yl)benzene (hereafter noted bpyp) and 1,4-bis(1-imidazoly)benzene (hereafter noted bib) (Scheme 1) to connect with POMs clusters and copper atoms in order to construct POMOF compounds with different fold interpenetrated framewotk, more especially, compound **1** exhibits a three-fold interpenetrated frameworks, where the two-fold in **2** and none interpenetrated in **3** (Scheme 1). Furthermore, we investigated their photocatalytic activities about the decomposition of Rhodamine B.

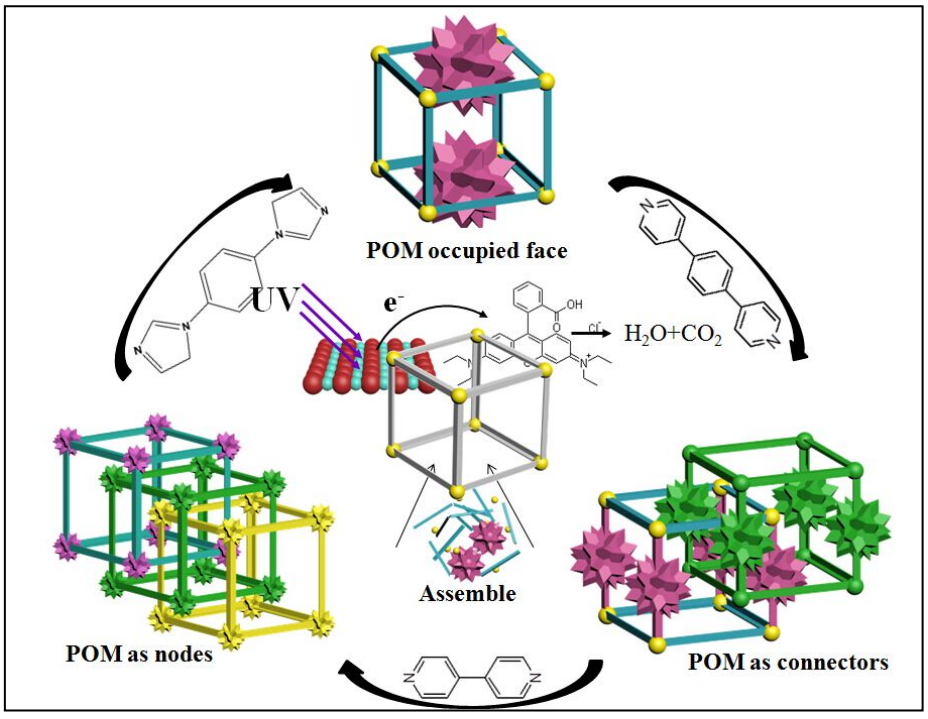

Scheme 1 Schematic representation of POMOFs with different interpenetrated folds and their photocatalytic activities about the decomposition of Rhodamine B.

Experimental Section

General methods and materials All reagents were purchased commercially and used without further purification. Elemental analysis (C, H, N and Cu) were performed on a Perkin-Elmer 2400 CHN Elemental Analyzer and on a Leaman inductively coupled plasma (ICP) spectrometer. The IR spectra were obtained on an Alpha Centaurt FT/IR spectrometer with KBr pellet in the 400-4000 cm^{-1} region. The XPRD patterns were obtained with a Rigaku D/max 2500V PC diffractometer with Cu-Kα radiation, the scanning rate is $4°.s^{-1}$, 2θ ranging from 5-40°. UV-Vis adsorption spectra were recorded on a 756 CRT UV-Vis spectrophotometer.

Synthesis of $[Cu_2(bipy)_2][H_2SiW_{12}O_{40}]\cdot(bipy)$ (1). A mixture of $H_4[SiW_{12}O_{40}]$ (300 mg), bipy (80 mg), $Cu(NO_3)_2$ (160 mg) and $(CH_3)_4NOH$ (4 mmol) was dissolved in 10 ml of distilled water at room temperature. The pH value was adjusted to about 2.4 with 2.0 M HCl, then the solution was kept at 170°C for 4 days. The reactor was then slowly cooled down to room temperature over a period of 13 h. Dark red block crystals of **1** were obtained (32% yield based on Cu). Elemental analysis found: C 10.34, H 0.81, N 2.38, Cu 3.68%; calc. for **1**, $C_{30}H_{26}N_6Cu_2SiW_{12}O_{40}$ (3471.82): calcd. C 10.37, H 0.75, N 2.42, Cu 3.69%.

Synthesis of $[Cu(bpyb)_2(H_2O)_2][H_2SiW_{12}O_{40}]\cdot(bpyb)$ (2). A mixture of $H_4[SiW_{12}O_{40}]$ (300 mg), bpyb (80 mg), $Cu(NO_3)_2$ (160 mg) and $(CH_3)_4NOH$ (4 mmol) was dissolved in 10 ml of distilled water at room temperature. The pH value was adjusted to about 2.9 with 2.0 M HCl, then the solution was kept at 170°C for 4 days. The reactor was then slowly cooled down to room temperature over a period of 13 h. Blue block crystals of **2** were obtained (42% yield based on Cu). Elemental analysis found: C 15.66, H 1.23, N 2.27, Cu 1.72%; calc. for **1**, $C_{48}H_{42}N_6CuSiW_{12}O_{42}$ (3672.42): calcd. C 15.68, H 1.14, N 2.29, Cu 1.74%.

Synthesis of $[Cu(bib)][H_2SiW_{12}O_{40}]\cdot(bib)\cdot 2H_2O$ (3). A mixture of $H_4[SiW_{12}O_{40}]$ (300 mg), bib (80 mg), $Cu(NO_3)_2$ (160 mg) and $(CH_3)_4NOH$ (4 mmol) was dissolved in 10 ml of distilled water at room temperature. The pH value was adjusted to about 2.8 with 2.0 M HCl, then the solution was kept at 170°C for 4 days. The reactor was then slowly cooled down to room temperature over a period of 13 h. Green block

crystals of **3** were obtained (28% yield based on Cu). Elemental analysis found: C 8.46, H 0.81, N 3.27, Cu 1.87%; calc. for 1, $C_{24}H_{26}N_8CuSiW_{12}O_{42}$ (3396.20): calcd. C 8.48, H 0.76, N 3.30, Cu 1.88%.

Crystallographic data collections and refinement.

X-ray single crystal diffraction data for compounds **1** to **3** were collected on a Bruker Apex-II CCD detector using graphite monochromatized Mo Kα radiation (λ= 0.71073 Å) at room temperature. Routine Lorentz and polarization corrections were applied. The structures were solved by direct methods and refined on F^2 by full-matrix least squares using the SHELXTL-97 program package on a Legend computer.[13] All of the non-hydrogen atoms except some disordered atoms were refined with anisotropic thermal displacement coefficients. The positions of hydrogen atoms on carbon atoms were calculated theoretically. During the refinement, the command "isor" was used to restrain the non-H atoms with ADP and NPD problems, which led to relative high restraint values: 178 for **1**. The command "ISOR" was used to refine atoms C1, C3, C5, C12, C14, C15, N2, N3, O1, O2, O3, O4, O5, O7, O8, O15, O16, and O17. Additionally, restraint command "DFIX" and "DANG" was used to amend the pyridine. The detailed crystallographic data and structure refinement parameters are summarized in Table 1. Select bond distances for compound **1** to **3** are listed in Table S1 to S3. These three compounds for the structures reported in this paper have been deposited in the Cambridge Crystallographic Data Center with CCDC numbers 1011203 for **1**, 1011204 for **2**, and 1011205 for **3**.

Table 1 Crystallographic and structural refinement data of **1** to **3** at 293 K

Compounds	**1**	**2**	**3**
Chemical formula	$C_{30}H_{26}N_6Cu_2SiW_{12}O_{40}$	$C_{48}H_{42}N_6CuSiW_{12}O_{42}$	$C_{24}H_{26}N_8CuSiW_{12}O_{42}$
CCDC no.	1011203	1011204	1011205
Formula weight	3471.82	3672.42	3396.20
Temperature (K)	293	293	293
Wavelength (Å)	0.71069	0.71069	0.71069
Crystal system	monocline	monocline	monocline
Space group	*P 21/c*	*C 2/m*	*C 2/c*

a(Å)	11.622(5)	16.044(5)	24.737(5)
b(Å)	22.213(5)	21.276(5)	10.601(5)
c(Å)	11.896(5)	11.001(5)	20.038(5)
α(°)	90.00	90.00	90.00
β(°)	112.74	110.46	99.41
γ(°)	90.00	90.00	90.00
V(Å3) / Z	2832.4(18) /2	3518(2) /2	5184(3) /4
Density ($g \cdot cm^{-3}$)	4.144	3.507	4.344
Abs coeff. (mm^{-1})	25.122	19.947	27.045
F(000)	3116.0	3298	5948
Index range	-13<=h<=13 -26<=k<=25 -13<=l<=14	-19<=h<=19 -25<=k<=25 -12<=l<=13	-29<=h<=26 -12<=k<=10 -23<=l<=22
Reflns collected	10642	12233	8583
Independent reflns	4992	3186	4545
R(int)	0.0572	0.0436	0.0478
Data/restraints/parameters	4992/178/430	3186/28/319	4545/48/399
Goodness-of-fit on F^2	1.198	1.107	1.127
Final R indices [I > 2δ(I)]	R_1= 0.0943, wR_2= 0.2013	R_1= 0.0423, wR_2= 0.1203	R_1= 0.0455, wR_2= 0.1095
R indices (all data)	R_1= 0.1126, wR_2= 0.2108	R_1= 0.0573, wR_2= 0.1424	R_1= 0.0550, wR_2= 0.1163

$R_1 = \Sigma(||F_0|-|F_c||)/\Sigma|F_0|$, $wR_2 = \Sigma w(|F_0|^2-|F_c|^2)^2/\Sigma w\,(|F_0|^2)^2]^{1/2}$

Results and discussion

As described in the experimental section, during the syntheses of the title compounds, the use of $(CH_3)_4NOH$ species was necessary for the isolation of the compounds. It may be explained that $(CH_3)_4NOH$ may play a role of the mineralization. Bond valence sum calculations [14] for the compounds show that all tungsten atoms are in +VI oxidation states, and copper atoms are in +I oxidation states for **1** and +II for **2** and **3**, which was confirmed by crystal color, charge neutrality and coordination environments valence sum calculations. The compounds crystallize in the monoclinic space group *P 21/c*, *C 2/m*, and *C 2/c* for **1**, **2**, and **3** respectively.

Structural Description

Structure of $[Cu_2(bipy)_2][H_2SiW_{12}O_{40}]\cdot(bipy)$ (1). A single-crystal X-ray diffraction

study performed on compound **1** reveals the formation of a 2D six-connected network that crystallizes in the space group *P21/c*. As shown in Fig. 1a, the asymmetric unit comprises one and a half of the bipy molecules, a half of $\{SiW_{12}\}$ cluster and one Cu atom. Each Cu(I) atom is coordinated by two N atoms from two bipy molecules and one O atom from the $\{SiW_{12}\}$ cluster to furnish a T-shape coordination geometry (Fig. S1a). The bond distances are 1.936 Å for Cu1-N1 and 1.939 Å for Cu1-N2. Each $\{SiW_{12}\}$ cluster acts as a bidentate inorganic ligand coordinating with two Cu centers (Fig. S1b). Additionally, there are two kinds of crystallographic independent bipy ligands: one linking with Cu atoms is named as L1 (Fig. S1c) and another is isolated as L2.

The structure of compound **1** can be described overall as three-fold interpenetrated POMOFs based on the ***pcu*** topology. Each ***pcu*** framework is constructed from $\{SiW_{12}\}$ clusters as nodes and Cu atoms and bipy ligands as connectors. More specifically, Cu centers and L1 molecules connected each other forming the 1D chains, which was further connected by $\{SiW_{12}\}$ clusters forming the 2D parallelogram-like fragment (Fig.1b and Fig.S2). The distances are 15.504 Å for Si-Si and the angles are 88.49 ° for Si-Si-Si. Two parallelogram-like fragments are then linked with each other by the connectors (L2) *via* the N3-O20 hydrogen bond (2.826 Å) to give a perfectly cubic-like framework with ***pcu*** topology (Fig. 1c and Fig. S3). Interestingly, due to the large porous of the whole net (Fig.1d) and to support the stability of the structure, three identical ***pcu*** frameworks interpenetrate one another to achieve the three-fold interpenetrated structure architecture (Fig. 1e and Fig. S4). To our knowledge, this is the first example with the three-fold interpenetrated features constructed by POM-based metal-organic hybrid with ***pcu*** topology.

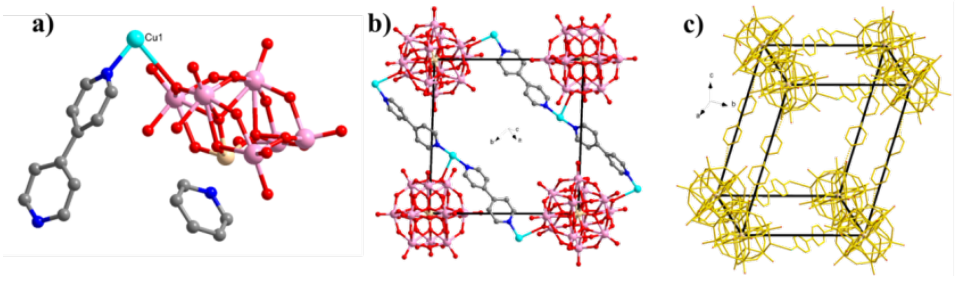

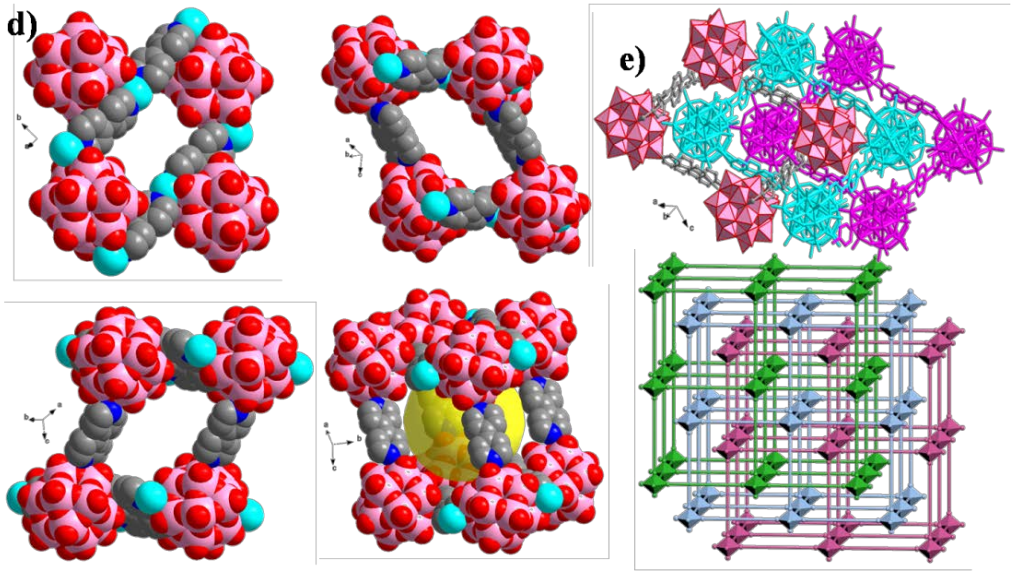

Fig. 1 a) Ball/stick representation of the unit cell of compound **1**; the subunit of b) 2D parallelogram-like fragment and c) ***pcu*** topology; d) the large porous in single net of **1** from different directions; e) the topology of 3-fold interpenetrated structure.

Structure of $[Cu(bpyb)_2(H_2O)_2][H_2SiW_{12}O_{40}]\cdot(bpyb)$ (2). A single-crystal X-ray diffraction study performed on compound **2** reveals the formation of a 2D six-connected network that crystallizes in the space group *C2/m*. As shown in Fig.2a, the asymmetric unit comprises one bpyb molecules, one-third $\{SiW_{12}\}$ cluster, one-third Cu atom and crystal water. Each Cu(II) ions exhibits octahedron coordination geometry defined by four N atoms from four bpyb molecules and two waters (Fig. S5). The bond distances are 2.038 Å for Cu-N and 2.327 Å for Cu-O, and all the distances are in the normal range. Furthermore, there are two crystallographic independent bpyb molecules: L1 shows a bidentate ligand with linear geometry coordinated by two Cu1 atoms (Fig. S5) and L_2 is isolated. Different from compound **1**, the $\{SiW_{12}\}$ clusters in **2** is isolated.

The structure of compound **2** comprises the POM-pillared MOFs, which can be described overall as two-fold interpenetrated frameworks with the ***pcu*** topology. Each ***pcu*** framework is constructed from Cu centers as nodes and $\{SiW_{12}\}$ clusters and bpyb molecules as connectors. First, each Cu(II) cation links with four bpyb molecules and two waters showing the 6-connected octahedron nodes, and each bpyb ligand as bidentate model linking with two Cu atoms, which form the square nearly MOFs with the very large cavities with dimensions of ca. 22.242 × 22.242 Å *via* Cu

and Cu ions (Fig. 2b and Fig. S6). Moreover, POMs play an important role in this compound and conduct the formation of this whole ***pcu*** net. Namely, each POM connects two Cu-organic polymers *via* the hydrogen bond between O9-O1W (2.835 Å) (Fig. 2c and Fig. S7) resulting in the formation of the ***pcu*** framework (Fig. 2d and Fig. S8). Interestingly, because the void space in the single net is so large that two identical ***pcu*** nets interpenetrate each other to achieve the two-fold interpenetrated structure architectures (Fig. 2e). Note that there are porous between the two interpenetrated frameworks, which are occupied by isolated bpyb molecules (Fig. S9).

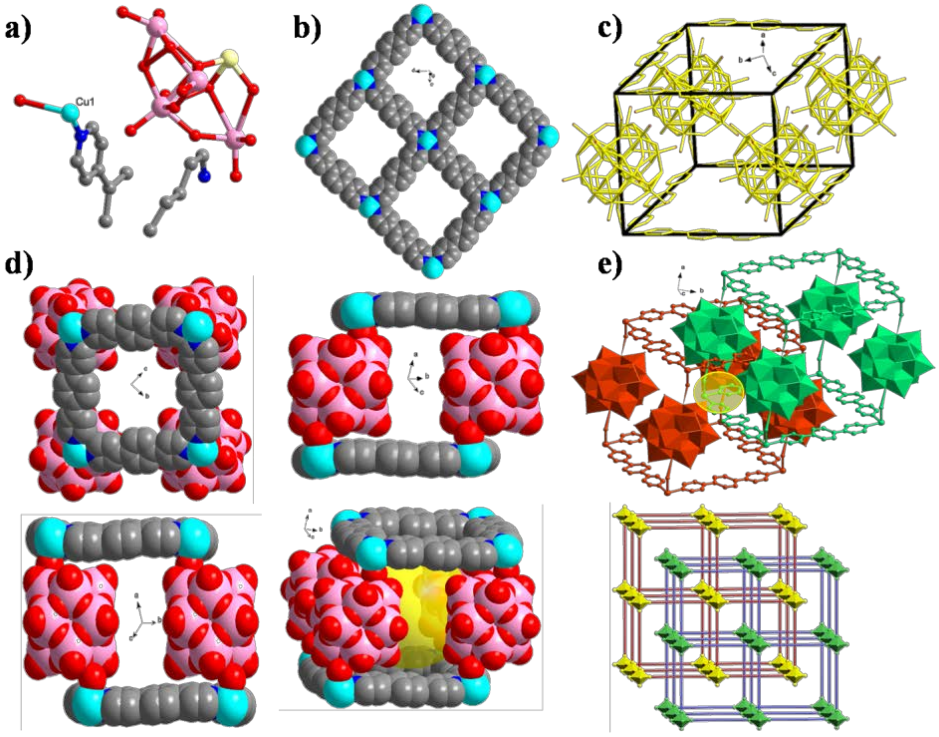

Fig. 2 a) Ball/stick representation of the unit cell of the compound **2**; b) stack of the square nearly MOFs; c) the subunit of *pcu* topology of **2**; d) the large porous in single net of **2** from different directions; e) the topology of 2-folds interpenetrated structure.

Structure of [Cu(bib)][$H_2SiW_{12}O_{40}$]·(bib)·$2H_2O$ (3). A single-crystal X-ray diffraction study performed on compound **3** reveals the formation of a 3D six-connected network that crystallizes in the space group *C2/c*. As shown in Fig. 3a, the asymmetric unit comprises one bib molecule, a half of {SiW_{12}} cluster, a half of Cu atom and one crystal waters. Each Cu(II) cation exhibits octahedron coordination geometry defined by four O atoms from four {SiW_{12}} clusters and two N atoms from two bib molecules. The bond distances are 2.121-2.314 Å for Cu-O and 1.943Å for Cu-N. All the distances are in the normal range. Furthermore, there are two

crystallographic independent bib molecules: L1 links with two Cu centers in *trans*-mode; L2 is isolated in this compound. Additionally, each $\{SiW_{12}\}$ cluster as connector link with four Cu centers with the Cu1-O20 and Cu1-O3 bonds (Fig. S10).

Different from compounds **1** and **2,** the structure of compound **3** can be described as a single ***pcu*** network. First, the adjacent Cu centers are held together *via* the POMs to construct the inorganic mesh-like nets (Fig. 3b and Fig. S11). Furthermore, each L1 molecule links two Cu atoms from different nets forming the whole organic-inorganic hybid compound in a *trans*- mode (Fig.3c and Fig. S12 and Fig.S13), which indicates that the *trans*-coordination mode can improve the stability of the overall structure. Note that the whole 3D ***pcu*** structure constructed by the inorganic mesh-like nets and the Cu-L1 chains possess a large porous (Fig. 3d &e), which is smaller than that of compound **1** and **2**, so compound **3** exhibit a non-interpenetrated ***pcu*** network, maybe because the POMs occupy the face of the nets, which prevents the formation of the interpenetration features.

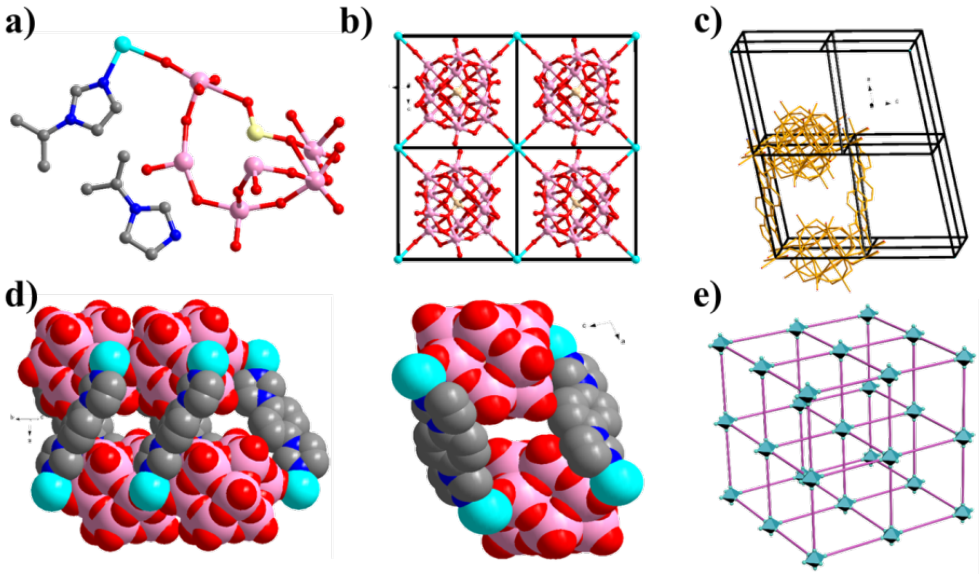

Fig. 3 a)Ball/stick representation of the unit cell of the compound **3**; b) ball/stick representation of the inorganic mesh-like nets; c) the ***pcu*** topology of **3**; d) the large porous in single net of **3** from different directions; e) structure of none interpenetrated.

Influence of organic molecule on the structure of the compounds. It is obvious that the type of organic molecules play a significant role in determining the structure of the resultant compounds shown in Fig. 4. Compound **1** was synthesized by using bipy ligand, and **2** and **3** by using bpyb and bib ligand, respectively. During the

investigation of network, we find that the length and the coordination angle of the ligand play an important role in construction of the final structure. In compound **1**, the bipy molecule (7.043 Å) are shorter than the $\{SiW_{12}\}$ cluster (10 Å), which leads to the POMs arranging two sides of the Cu-bipy chains, and the pillared L2 molecules can only connected to POMs clusters *via* the hydrogen bonds. The above reasons cause the $\{SiW_{12}\}$ clusters as the vertexes to form the ***pcu*** lattice and giving the large cavity (16 Å x 31 Å), which leading to a three-fold interpenetrated structure. When the length of the ligand is increased, the bpyb molecule (11.331 Å) is longer than that of $\{SiW_{12}\}$ cluster, them a 2D metal-organic polymer is obtained, in which the $\{SiW_{12}\}$ clusters are located exactly. Furthermore, the $\{SiW_{12}\}$ clusters as pillars link to the Cu centers forming the ***pcu*** lattice with Cu centers as vertex and giving the large cavity (11 Å x 11 Å). As a result, the two-fold interpenetrated structure is formed. When the bib molecule replaces the bpyb molecule in compound **3**, only one single ***pcu*** net is remained, which may be explained as the guiding function of the bib ligands. Firstly, the bib molecule coordinates with Cu centers in *trans*- mode with the angle of 160 °, which is different from that of the bipy and bpyb molecules (180 °). Secondly, the length of bib molecule (9.717 Å) is little shorter than the diameter of $\{SiW_{12}\}$ cluster, which prevents the formation of the Cu-bib layers like compound **2**, but only forms the Cu-bib chains. As a result, the $\{SiW_{12}\}$ clusters link with the Cu-bib chains forming the ***pcu*** lattice, and the $\{SiW_{12}\}$ clusters occupy the face of the nets. Due to the reasons, a single ***pcu*** net is formed. This result indicates that the controllable and designable length and coordination modest of organic molecules can greatly control the interpenetrated folds in POM-based metal-organic frameworks.

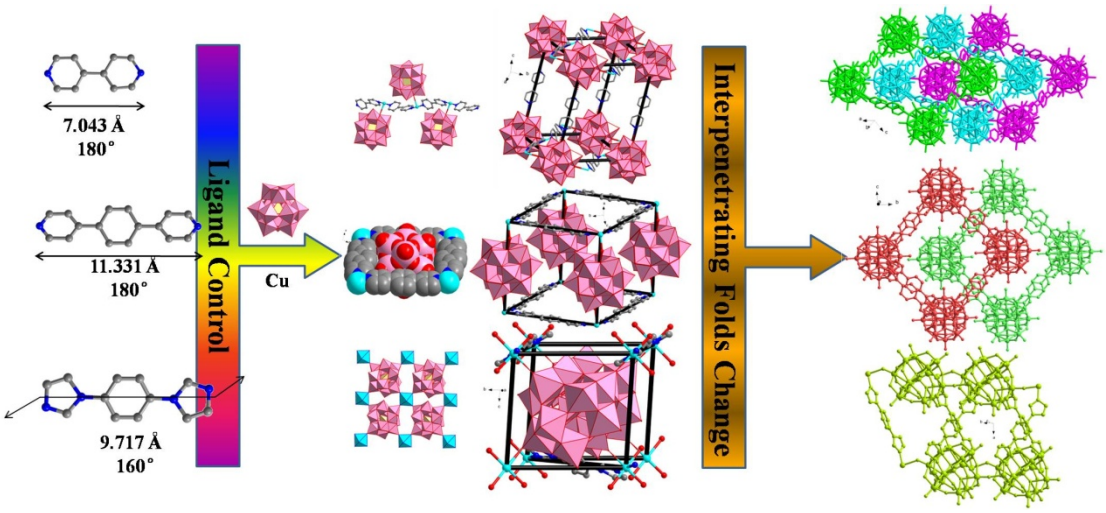

Fig. 4 Representations of the strategy for the control interpenetrated folds *via* ligand molecules.

XRPD Pattern and IR Spectra

The XPRD patterns for the compounds **1-3** are presented in the Fig. S14. The diffraction peaks of both simulated and experimental patterns match well, thus indicating that the phase's purity of the compounds is good. The difference in reflection intensities between the simulated and the experimental patterns are due to the different orientation of the crystals in the powder samples. The IR spectra of compounds **1-3** are shown in Fig. S15. Characteristic bands at 958, 906, 786 cm^{-1} for **1**, 971, 913 and 783 for **2**, 978, 920 and 798 for **3** are attributed to ν (W=O), ν (Si-O), and ν (W-O-W) vibrations, respectively. Band in the regions of 1620-1205 cm^{-1} are attributed to the organic ligands.

Photocatalysis properties

The use of POMs as photocatalysts to decompose waste organic molecules so as to purify the water resources has attracted great attention in recent years. The introduction of transition-metal complexes as functional groups into POMs can enrich their potential applications. Herein, to investigate the photocatalytic activities of compounds **1-3** as catalysts, the photodecomposition of Rhodamine-B (RhB) is evaluated under UV light irradiation through a typical process (see Supplementary Information). The photodegradation of RhB assisted by compounds **1-3** and their matrix ($(NBu_4)_4[SiW_{12}O_{40}]$) are shown in Fig.5. RhB has a major absorption peak at 554nm, which decreases from 1.13 to 0.55 for **1**, from 0.964 to 0.292 for **2**, from

0.968 to 0.523 for **3**, and from 0.774 to 0.508 for $(NBu_4)_4[SiW_{12}O_{40}]$. After irradiation compounds **1**-**3** for 360 min, the photocatalytic decomposition rate, defined as $1-C/C_0$, is 51.3% for **1**, 69.7% for **2** and 46.2% for **3**. In contrast, the photocatalytic decomposition rate using $(NBu_4)_4[SiW_{12}O_{40}]$ as catalyst is 35.04 % after UV light irradiation of 360 min.

The photocatalytic mechanisms may be deduced as follows: during photocatalytic reaction, ($*\{SiW_{12}\}$) abstract electrons from H_2O molecules and hold the electrons (reaction 1 and 2). The reduced POM ($\{SiW_{12}\}^-$) is quite stable but rapidly re-oxidized in the presence of O_2 through reaction 3, and the main function of O_2 in POM reactions seems to be the reoxidation (regeneration) of the catalyst.[15] The reoxidation (reaction 3) accompany the generation of superoxides. These cycles occur continuously while the system is exposed to the UV light.[16] Furthermore, the RhB dye is also excited by UV light to generate *RhB molecule as reaction 4. Finally, after several of photo-oxidation, the degradation of RhB dye by the hydroxyl radicals and the superoxides occurs [17] (reaction 5).

$$\{SiW_{12}\} + h\nu \rightarrow * \{SiW_{12}\} \quad (1)$$

$$* \{SiW_{12}\} + H_2O \rightarrow \{SiW_{12}\}^- + H^+ + OH^{\cdot} \quad (2)$$

$$\{SiW_{12}\}^- + O_2 \rightarrow \{SiW_{12}\} + O_2^- \quad (3)$$

$$RhB + h\nu \rightarrow *RhB \quad (4)$$

$$*RhB \xrightarrow{OH^{\cdot}+O_2^-} CCO + CO_2 + H_2O \quad (5)$$

Where CCO= colorless compounds organic.

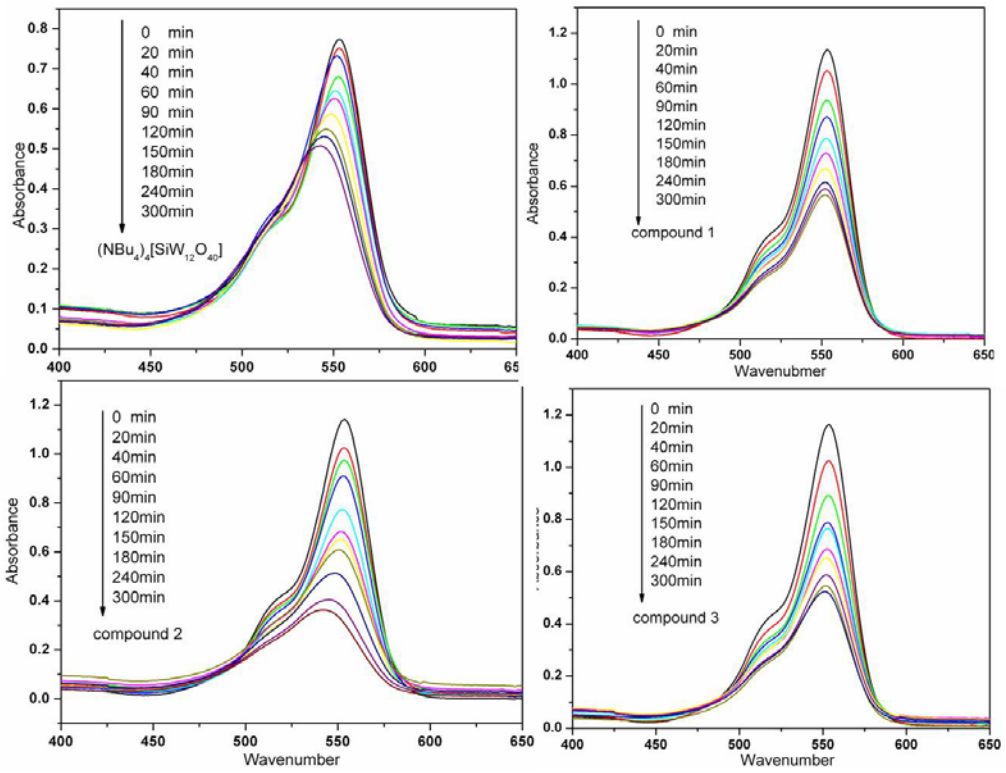

Fig.5 UV–vis adsorption changes observed for RhB solutions as a function of UV light irradiation time in the presence of compounds **1-3** and $(NBu_4)_4[SiW_{12}O_{40}]$as catalyst..

Conclusions

In summary, we have prepared and characterized three new POMOFs containing three-fold interpenetrated, two-fold interpenetrated, and non-interpenetrated net for compounds **1**, **2**, and **3**, respectively. It is interesting that the three POMOFs possess the same ***pcu*** topology with POMs occupying the vertex, arris and face of *pcu* lattice, respectively. It can be concluded that the type of organic molecules play an important role in forming the final products. This work represents the first example on ligand molecule controlling over the degree of interpenetrated system in POMOFs. So the work provides not only novel examples of POMOFs with different fold interpenetration, but also a new strategy for control of the interpenetrated system.

Acknowledgements

This work is financially supported by the National Natural Science Foundation (Grant Nos. 21271089, 21272061), the Natural Science Foundation (No.B201214) and the training program for New Century Excellent Talents in universities (1253-NCET-022) and Postdoctoral Foundation in Heilongjiang Province.

Appendix A. Supplementary data

Crystallographic data and CCDC can be obtained free of charge from the Cambridge Crystallographic Data Centre via www.ccdc.cam.ac.uk/data_request/cif. Tables of selected bond lengths (Å) , bond angles (deg) and Figures, IR, XRPD for compound are provided in supporting information.

References

(1) (a) M. F. Joseph, C. Wang, S. Liu, W. B. Lin, *Angew. Chem., Int. Ed.* 2011, **50**, 8674; (b) S. Subramanian, M. Zaworotko, Coord. *Chem. Rev.* 1994,**127**, 357; (c) S. R. Batten, R. Robson, *Angew. Chem., Int. Ed.* 1998, **37**, 1460; (d) D. Liu, J. P. Lang, B. F. Abrahams,*J. Am. Chem. Soc.* 2011,**133**, 11042; (e) A. Filipe, P. Almeida, K. Jacek, M. F. Sérgio, P. C. João, A. S. José , R. João,*Chem. Soc. Rev.* 2012, **41**, 1088.

(2) (a) J. Seo, R. Matsuda, H. Sakamoto, C. Bonneau, S. Kitagawa, *J. Am. Chem. Soc.* 2009, **131**, 12792; (b) T. K. Maji, G. Mostafa, R. Matsuda, S. Kitagawa, *J. Am. Chem. Soc.* 2005, **127**, 17152; (c) E. Q. Procopio, F. Linares, C. Montoro, V. Colombo, A. Maspero, E. Barea, J. A. R. Navarro, *Angew. Chem. Int. Ed.* 2010, **49**, 7308; (d) B. Xiao, P. J. Byrne, P. S. Wheatley, D. S. Wragg, X. Zhao, A. J. Fletcher, K. M. Thomas, L. Peters, J. S. O. Evans, J. E. Warren, W. Zhou, R. E. Morris, *Nature Chem.* 2009, **1**, 289.

(3) (a) Brigitte Nohra, Hani El Moll, L. Marleny Rodriguez Albelo, Pierre Mialane, Jé rôme Marrot, Caroline Mellot-Draznieks, Michael O'Keeffe, Rosa Ngo Biboum, Joël Lemaire, Bineta Keita, Louis Nadjo and Anne Dolbecq, *J. Am. Chem. Soc.* 2011, **133**, 13363–13374; (b) C. L. Hill, *Chem. Rev.* 1998, **98**, 1; (c) K. Fukaya, T. Yamase, *Angew. Chem. Int. Ed.* 2003, **42**, 654; (d) A. Müller, S. Q. N. Shah, H. BPgge, M. Schmidtmann, *Nature*, 1999, **397**, 48; (c) L. Xu, M. Lu, B. Xu, Y. Wei, Z. Peng, D. R. Powell, *Angew. Chem. Int. Ed.* 2002, **41**, 4129; (e) P. Kögerler, L. Cronin, *Angew. Chem. Int. Ed.* 2005,**44**, 844; (f) E. Coronado, C. J. Gómez-Garca, *Chem. Rev.* 1998, **98**, 273; (g) Dong-Ying Du, Jun-Sheng Qin, Ting-Ting Wang, Shun-Li Li, Zhong-Min Su, Kui-Zhan Shao, Ya-Qian Lan, Xin-Long Wang and En-Bo Wang, *Chem. Sci.* 2012, **3**, 705; (h) P. Wang, X. Wang, G. Zhu, *Electrochim.*

Acta. 2000, **46**, 637.

(4) (a) H. Y. An, E. B. Wang, D. R. Xiao, Y. G. Li, Z.M. Su, L. Xu, *Angew. Chem., Int. Ed.* 2006, **45**, 904; (b) H.Y. Liu, H. Wu, J. Yang, Y.Y. Liu, J.F. Ma, H.Y. Bai, *Cryst. Growth Des.* 2011, **11**, 1786; (c) F. J. Ma, S. X. Liu, C.Y. Sun, D.D. Liang, G.J. Ren, F. Wei, Y.G. Chen, Z.M. Su, *J. Am. Chem. Soc.* 2011, **133**, 4178; (d) C.Y. Sun, S.X. Liu, D.D. Liang, K.Z. Shao, Y.H. Ren, Z.M. Su, *J. Am. Chem. Soc.* 2009, **131**, 1883; (e) X. L.Wang, N. Li, A.X. Tian, J.Ying, T.J. Li, X. L. Lin, J. Luan, Y. Yang. *Inorg.Chem.* 2014, **54**, 7118; (f) J.Q. Sha, M.T. Li, J.W. Sun, P.F.Yan, G.Ming Li, L.Zhang, *J.Asia.Chemistry*, 2013, **8**, 2252.

(5) (a) J. He, Y. G. Yin, T. Wu, D. Li, X. C. Huang, *Chem. Commun.* 2006, 2845; (b) S. B. Choi, H. Furukawa, H. J. Nam, D. Y. Jung, Y. H. Jhon, A. Walton, D. Book, M. O'Keeffe, O. M. Yaghi, J. Kim, *Angew. Chem. Int. Ed.* 2012, **51**, 8791.

(6) (a) H. Wu, J. Yang, Z. M. Su, S. R. Batten, J. F. Ma, *J. Am. Chem. Soc.* 2011, **133**, 11406; (b) X. L. Wang, C. Qin, E. B. Wang, Y. G. Li, Z. M. Su, L. Xu and L. Carlucci, *Angew. Chem. Int. Ed.* 2005, **44**, 5824.

(7) (a) J. Zhang, L. Wojtas, R. W. Larsen, M. Eddaoudi, M. J. Zaworotko, *J. Am. Chem. Soc.* 2009, **131**, 17040; (b) J. Guo, G. Xu, G. Guo, *Chin. J. Chem.* 2012, **30**, 791.

(8) D. L. Long, R. J. Hill, A. J. Blake, N. R. Champness, P. Hubberstey, C. Wilson, M. Schroder, *Chem.–Eur. J.* 2005, **11**, 1384.

(9) (a) T. K. Prasad, M. P. Suh, *Chem.–Eur. J.* 2012, **18**, 8673; (b) S. Ma, D. Sun, M. Ambrogio, J. A. Fillinger, S. Parkin, H. C. Zhou, *J. Am. Chem. Soc.* 2007, **129**, 1858.

(10) (a) S. Ma, J. Eckert, P. M. Forster, J. W. Yoon, Y. K. Hwang, J.-S. Chang, C. D. Collier, J. B. Parise, H.-C. Zhou, *J. Am. Chem. Soc.* 2008, **130**, 15896; (b) S. Ma, D. Sun, M. Ambrgio, J. A. Fillinger, S. Parkin, H.-C. Zhou, *J. Am. Chem. Soc.* 2007, **129**, 1858; (c) O. Shekhah, H. Wang, M. Paradinas, C. Ocal, B. Schupbach, A. Terfort, D. Zacher, R. A. Fischer, C. Woll, *Nat. Mater.* 2009, **8**, 481; (d) T. K. Prasad, M. P. Suh, *Chem. Eur. J.* 2012, **18**, 8673.

(11) (a) X. L. Wang, D. Zhao, A. X. Tian and J. Ying, *CrystEngComm*. 2013, **15**, 4516;

(b) L. L. Fan, D. R. Xiao, E. B. Wang, Y. G. Li, Z. M. Su, X. L. Wang and J. Liu *Crystal Growth & Design* 2007, **7**, 592; (c) H. Y. Liu, H. Wu, J. F. Ma, Y. Y. Liu, J. Yang and J. C. Ma, *Dalton Trans*. 2011, **40**, 602 (d) S. T. Zheng and G. Y. Yang, *Dalton Trans*. 2010, **39**, 700.

(12) S. Kitagawa, R. Kitaura and S. Noro, *Angew. Chem., Int. Ed.* 2004, **43**, 2334.

(13) (a) G. M. Sheldrick, SHELX-97, Program for Crystal Structure Refinement, University of Göttingen, Germany, **1997**. (b) G. M. Sheldrick, SHELXL-97, Program for Crystal Structure Solution, University of Göttingen, Germany, **1997**.

(14) I. D. Brown, D. Altermatt, *Acta Crystallogy. Sect. B.* 1985, **41**,244.

(15) (a) H. Park, W. Choi, *J. Phys. Chem. B* 2003, **107**, 3885; (b) A. Mylonas, E. Papaconstantinou, *J. Photochem. Photobiol. A* 1996, **94**, 77; (c) A. Hiskia, E. Papaconstantinou, *Inorg. Chem.*1992, **31**, 163.

(16) E. Papaconstantinou, *Chem. Soc. Rev.*1989,*18*. 1.

(17) (a) L. S. Cavalcante, F. M. C. Batista, M. A. P. Almeida, A. C. Rabelo, I. C. Nogueira, N. C. Batista, J. A. Varela, M. R. M. C. Santos, E. Longobd, M. S. Li, *Advanced Powder Technology* 2013, **24,** 344; (b) L.S. Cavalcante, J.C. Sczancoski, N.C. Batista, E. Longo, J. A.Varela, M.O. Orlandi, *RSC Adv.* 2012, **2**, 6438.

Graphical abstract

Three different fold interpenetrating POMOFs were reported and the influence of the organic molecules on the degree of interpenetration of compounds is discussed.